Total Temperature Measurements Using a Rearward Facing Probe in Supercooled Liquid Droplet and Ice Crystal Clouds

Juan H. Agui,[1] and Peter M. Struk.[2]
NASA Glenn Research Center, Cleveland, OH, 44135, USA

and
Tadas P. Bartkus[3]
Ohio Aerospace Institute, Cleveland, OH, 44135, USA

This paper presents an analysis of local total temperature and humidity experimental measurement taken in atmospheric ice cloud flows. The measurements were obtained in a series of tests in NASA's Propulsion Systems Laboratory. The probe used in the tests is referred to as the Rearward Facing Probe which was designed to mitigate the contamination effects of ice accretion and ingestion into the probe. The data provided important insights in the interaction of the ice cloud and the atmospheric flow. For the majority of the test runs, small temperature drops in the range of 0.6 to 2.8 ºC and up to 1.5 g/kg of water vapor rise were found as a result of the interaction. Under certain very low temperature or high TWC conditions, the interaction with the cloud produced a warming of the airflow. A thermal model based on evaporative and convective heat transfer mechanisms between the spray droplets and the airflow showed good agreement with the experimental data. Detailed analyses of the response of the probe under various flow, thermodynamic, and cloud conditions, are provided in the paper.

I. Nomenclature

q_v	=	Evaporative heat flux [W/m^2]
q_c	=	Convective heat flux [W/m^2]
MVD	=	Median Volumetric Diameter [µm]
MMR	=	Mass Mixing Ratio [g/kg]
$\dot{m}_{water}$	=	water mass flow rate [kg/s]
P_{air}	=	Air pressure [kPa]
P_{pl}	=	Plenum static pressure [kPa]
RH	=	Relative humidity [%]
T_{air}	=	Air temperature [ºC]
T_0	=	Total Temperature [ºC]
$T_{0,RFP}$	=	Total Temperature taken with the Rearward Facing Probe [ºC]
T_p	=	Particle temperature [ºC]
T_{pl}	=	Plenum static temperature [ºC]
T_w	=	Water temperature [ºC]
TWC	=	Total Water Content [g/m^3]
TWC_{target}	=	Target Total Water Content [g/m^3]
v_{air}	=	Air velocity [m/s]
v_p	=	Particle velocity [m/s]

[1] Aerospace Engineer, Thermal Systems Branch, 21000 Brookpark Road, AIAA Member. [2] Aerospace Engineer, Icing Branch, 21000 Brookpark Road, AIAA Senior Member.
[3] Senior Research Associate, Icing Branch, 21000 Brookpark Road, AIAA Member.

II. Introduction

Ice accretion can form inside aircraft engines under certain atmospheric conditions leading to engine performance losses and anomalies. Mason et al.[1] has proposed that the main cause of engine icing at high altitudes is due to the partial melting of ice crystals ingested into the warm engine core that later refreeze onto internal components. This phenomenon is thought to be associated with multiple observed incidents of engine rollback, flameout, and even the cause of internal engine damage. Therefore, there is a keen interest in studying the engine icing phenomenon in order to identify and understand the prevailing conditions and responsible mechanisms that promote this phenomenon. For this purpose NASA Glenn Research Center's Propulsion Systems Laboratory (PSL), Test Cell #3, is one of only a few global facilities that is capable of simulating the ice-laden flight-altitude flow conditions required to investigate icing related performance-losses in jet engines.

The PSL generates concentrated ice cloud flows consisting of fully or partially frozen ice crystals that are formed as the cloud proceeds downstream from the facility's plenum section and subsequently impinges on test articles and probes used for investigations. These conditions set up a very challenging environment in which to perform some traditional wind-tunnel measurements. In particular, standard temperature probes are susceptible to ice accretion on the probe inlets and on the internal sensors, especially under high ice-water conditions. To overcome these challenges a total temperature probe is being developed and tested in-house [2, 3]. The Rearward Facing Probe (RFP) is similar in concept to a probe developed by the National Research Council of Canada which was designed to mitigate the contamination effects brought on by the icing clouds by preventing the ingestion of ice crystals and water droplets at the probe inlet [4]. Additionally, the gas sampled by the probe can be used to provide simultaneous humidity measurements.

Total temperature measurements are significant in atmospheric flows since they quantify the flow's inertial and thermal energy. When exposed to the ice cloud, the interaction between the main flow and the icing cloud can promote a thermal exchange, including possible phase change, between the ice crystals and water droplets and the gas phase. This can lead to an alteration of the local static and total temperatures of the flow. Bartkus et al. [5, 6] reported on both experimental data obtained in the PSL and numerical data obtained using a thermal model that demonstrated changes in air temperature as a result of the thermal exchange with the icing cloud.

This paper will provide an analysis of recently obtained data taken with the RFP in a series of ice cloud calibration and characterization tests performed in the PSL (see Ref. [7] for more details on these set tests). The probe's response to various flow and cloud conditions will be presented. The transient response of the probe to changes in conditions will be assessed. The probe's data will also help in interpreting the physical interaction between the icing cloud and the airflow. In addition, the data will be compared against the thermal model developed by Bartkus et al. This investigation will help to add to our understanding of the complex interaction between the icing cloud and airflow at high altitudes.

III. PSL Ice Cloud

The design and operation of the PSL is described in detail in Ref. [8]. Ice clouds are generated by a series of spray nozzles distributed in the plenum cross section upstream of the test section duct which introduce dispersed jets of water droplets into the main facility flow. The water droplets can either partially or fully freeze depending on thermodynamic flow conditions as they travel downstream into the test section. Under certain conditions, supercool liquid water droplets can also be generated and sustained during these tests. The size of the droplets are controlled by the flowrate of water and the atomizing air pressure. The water source can be either filtered, but non-demineralized (termed "city water"), or de-ionize (DI) water. The city water helps ensure nucleation sites for particle freezeout and is used for glaciated clouds while the DI water is used for supercooled water clouds. In addition, the spray bar water and atomizing air can be heated before being released through the nozzles. Typically, the spray bar water and atomizing air temperature were set to 7.2°C (45 °F) or 82.2°C (180 °F), for glaciated or supercooled water clouds, respectively. One of the prime objective of the cloud calibration tests was to explore the range of experimental parameters to produce supercooled water droplet clouds. Ref [7] provides more details on the test setup and results of this research effort. The droplets were generated with median volumetric diameters (MVD) ranging between 15 and 45 μm at varying total mass concentrations (or Total Water Content, TWC). Additional probes and techniques were used to measure the total water content, ice crystal particle sizes, and to image the cloud uniformity. Video imaging was used to monitor ice accretion on the probe.

IV. Rearward Facing Probe

A picture of the RFP is shown in Fig. 1. The RFP was constructed from 19 mm diameter stainless steel tubing with a 90º bend to form the inlet section. A small flow was induced through the probe using a vacuum source and flow

meter. The small flow passed through a commercial gas analyzer to measure the humidity level of the sampled air. Additionally, a smaller diameter extension tube was installed on the 19 mm diameter rearward facing probe inlet tip to prevent the ingestion of water that was observed to shed off of the probe body in previous tests. The RFP probe was mounted on a traversing support positioned just downstream of the exit test duct which allowed the probe to be positioned at various radial positions with respect to the circular exit duct. The RFP could also be fully retracted in between tests to melt and shed off any ice buildup on the probe body from previous tests. For the data presented in these tests, the probe was positioned 22.2 cm (8.75 inches) from the centerline of the flow. The reason the probe was positioned off-center was that present testing configuration involved multiple probes that did not allow for more than one probe at the tunnel centerline.

Recovery corrections are often applied to total temperature probes to account for non-isentropic deceleration of the internal probe flow. These corrections are typically dependent solely on flow speed. However, the transient response associated with the thermal mass of the probe can affect the results. Additional factors may also include air pressure and density, suction flow rate through the probe, relative humidity, and the presence of water or ice accretion on the probe body. The results presented in the next section have not been corrected for probe recovery or other effects like ice accretion on the probe. However, the recovery factor corrections are not required when reporting air total temperature changes at the same velocity. Ice accretion on the probe could cause a small offset in the measurement but was not quantified in this study. In this paper, measured temperature changes are reported between the period just prior to the cloud activation and the steady-state temperature reached after the cloud was activated. %. The accuracy of the resistance temperature detector (RTD) in the RFP is better than 0.5 ºC, and the accuracy of the temperature difference is further improved because the systematic error cancels out by differencing the measurement.

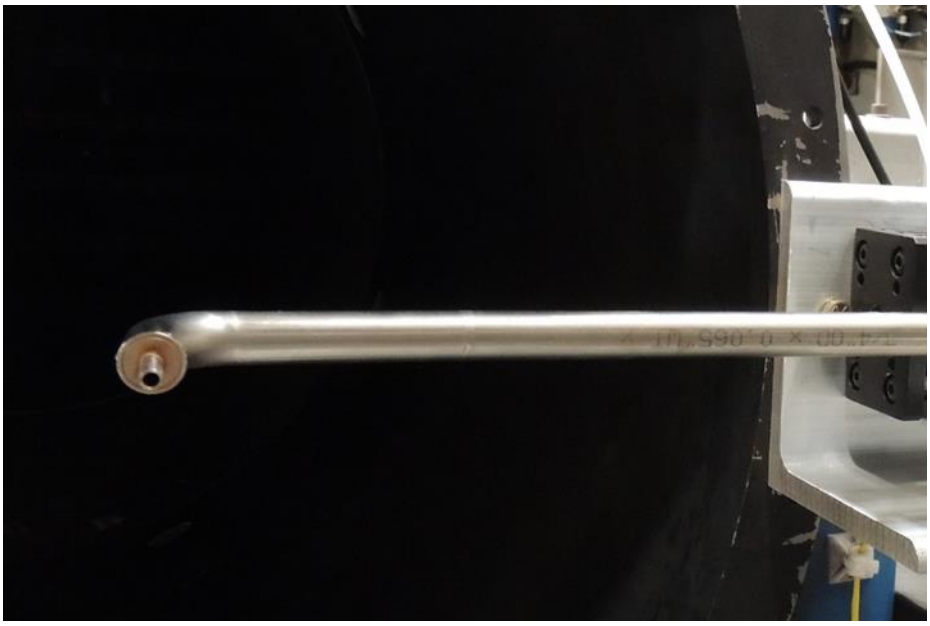

Figure 1: Picture of the Rearward Facing Probe installed on a traversing stand just downstream of the test duct exit.

V. Thermal model

It is hypothesized that the ice particles and water droplets of an icing cloud thermally interact with the flowing air causing the air temperature and humidity to change by the time the cloud and air masses reach the test section. An analytical thermal model was initially developed (Ref. [9]) to explain the observed changes in test conditions by coupling the conservation of mass and energy equations between the icing cloud and flowing air. The model will be referred to as the Bartkus thermal model. Modifications [5] and advancements [6] to the Bartkus model were made to simulate the condition in the PSL. The ultimate goal of the model is to better understand the complex interactions between the test parameters and have greater confidence in the conditions at the icing tunnel's test section. This model is used herein to explain the observed temperature changes for data presented in this section.

There are two competing heat transfer mechanisms that arise from this interaction, convective (q_c) and evaporative heat transfer (q_L) modes, as illustrated in Fig. 2. The two modes of heat transfer are initiated as soon as the warm droplets are introduced into the flow at a specified air temperature (T_{air}), pressure (P_{air}), and relative humidity (RH). For the cases reported in this paper the PSL generates altitude airflows at temperatures below 0 ºC while the sprayed droplets initially start at temperatures (T_p) close to the water temperature (7 - 82°C) in the spray. The droplets quickly cool down after some residence time in the flow. In the case of evaporative cooling, the latent heat energy of evaporation is drawn from the free stream airflow and thereby locally lowers the air temperature. The degree of evaporation depends on several variables including pressure, air temperature, water droplet size, and relative humidity. Conversely, condensation of water vapor on the droplet releases latent energy to the airflow resulting in warmer air temperatures. Convective heat transfer takes place throughout the interaction with the cloud. The large temperature difference, or gradient, between the water droplet and the airflow drives the convective heat transfer between droplet and the air. More details on these interactions and thermal mechanisms are provided in Ref [9].

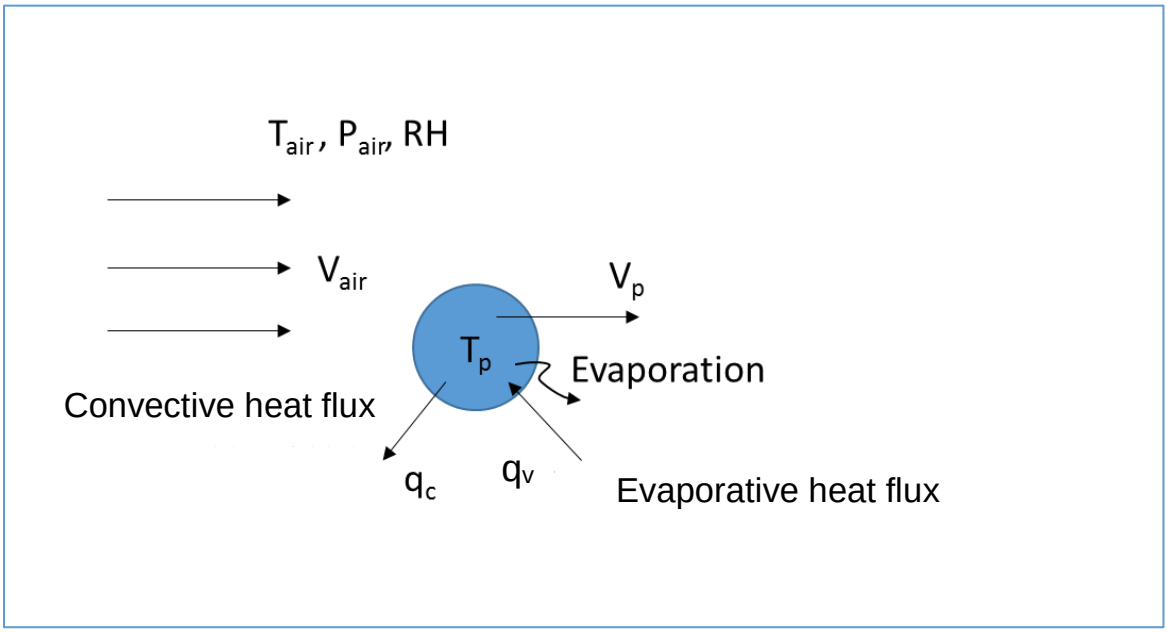

Figure 2: Droplet Thermal Model

VI. Results and Discussion

A recent set of cloud calibration tests at PSL produced an extensive data set that was used to investigate the interaction between the main atmospheric flow and the icing cloud. The facility offers a multitude of control parameters used to produce a large range of flows and ice cloud conditions, some of which are interdependent, requiring extensive data manipulation to extract parametric relations. The data obtained was reduced and parsed to obtain the time traced signals and average values during the different phases of the spraying events. It is important to note that the PSL cloud calibration tests were exploratory in nature with the goal of searching for particular types of ice crystal and droplet cloud conditions. To achieve this, the various facility variables were often times fine-tuned interdependently around a test point of interest in order to home in on the cloud condition. This led to a data set with small parametric variations around just a few points. The method used to effectively parametrize the data will be presented in the next section, Representative plots of the total temperature and humidity signals, represented by mass mixing ration (*MMR*), obtained rather with the RFP in the test section are shown in Fig. 3. The series of plots in Fig. 3 show the variations in measured temperature and water vapor (i.e. humidity) at the test section when the cloud was introduced. The quantities $\Delta T_{0,RFP}$ and ΔMMR are the difference of the 30-second average measured quantity just prior to cloud activation and another 30-second average just prior to the cloud coming off – the 30-second average values are shown as black horizontal lines in the plots of Fig. 3. The transient thermal response of the probe to changes in aerothermal flow conditions was of the order of 2 minutes as observed in Figs. 3a and 3c – this transient effect is believed to be due to the thermal time constant of the probe's metal body. The response was much quicker, of the order of seconds, to changes in humidity as seen in Fig. 3b – this time constant was characterized by the flow rate through the probe and distance to the gas analyzer. The plot of Fig. 3a shows the total temperature decreasing after

spray activation which was typical of most test cases. However, on several occasions, as shown in Fig. 3c, an inversion or increase of the total temperature after the spray activation was also observed. The humidity data provided in Fig. 3b is represented by the Mass Mixing Ratio (*MMR*) in units of: kg water vapor/kg of dry air. Detailed results and discussion of the major trends found with the two types of measurements are presented in the next two sections. First, the main parametric analysis comparing the test and modeling data in cases in which the ice cloud had a cooling effect on the atmospheric flow is discussed. The subsequent section will highlight a selected set of test points that gave rise to air temperature increases as a result of interaction with the cloud. Both sections provide discussion and analysis.

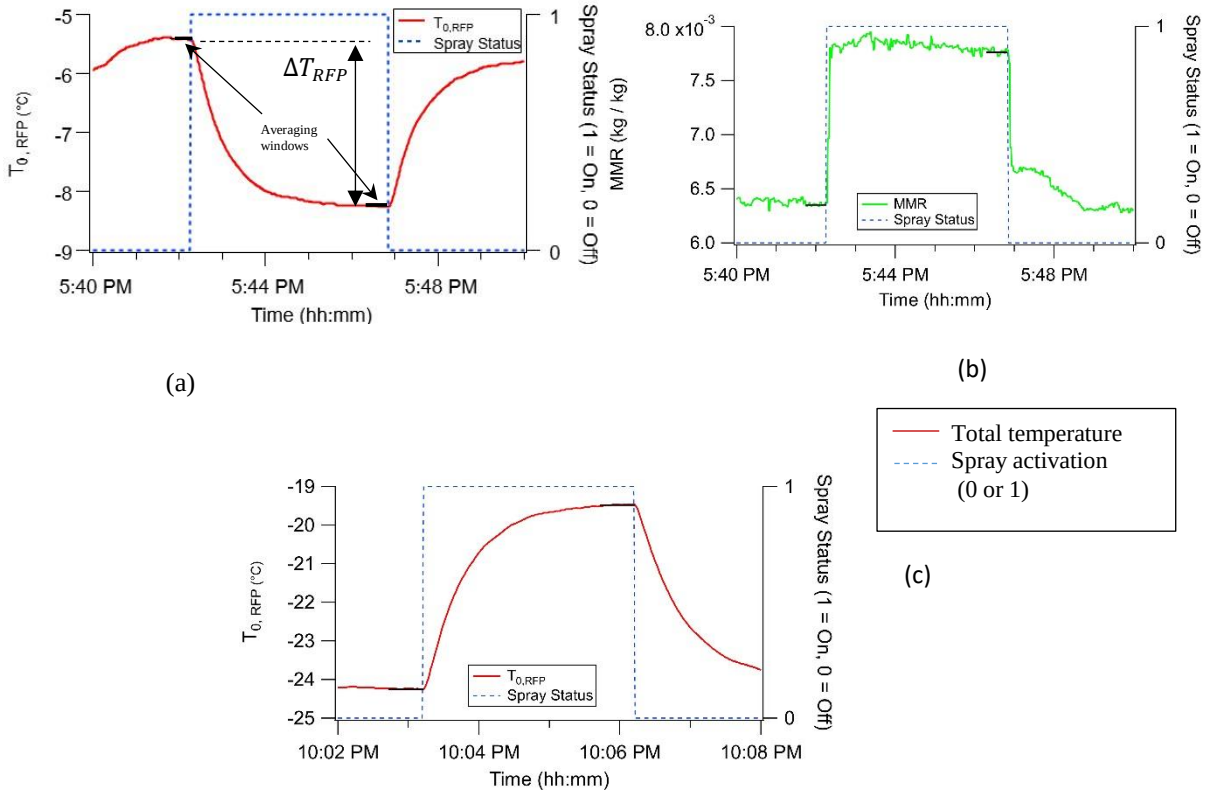

Figure 3: Plots of (a) Total temperature and (b) humidity signals obtained with the Rearward Facing Probe (RFP). (c) An alternate plot of total temperature showing the increase in total temperature after the spray was activated. The plot of Spray Status indicates when the cloud was inactive (0) or active (1) respectively.

A. Parametric Sweeps of Total Water Content

The large PSL cloud calibration data set was reduced and parametrized in terms of the facility's thermodynamic variables in the plenum section. The probe's measured data were plotted by sweeping through *TWC* values, providing a revealing and physically significant representation of the test data. The plotted *TWC* represents the target total water content (TWC_{target}), which assumes that all injected water reaches the PSL test section (i.e. no evaporation or condensation) and is uniformly distributed across the exit area. The value of TWC_{target} is calculated as the ratio of water mass flow rate to volumetric airflow rate at the test section and is calculated using Eq. (1) below. In this equation, $\dot{m}_{water}$ is the water mass flow rate, v_{air} is the air velocity at the tunnel test section, and *AREA* is the effective cloud area at the tunnel test section. The effective cloud area represents the area that the vast majority of the cloud exists, and does not necessarily cover the entire cross-sectional area of the tunnel. Boundary layer and which tunnel nozzles were used to generate the cloud, dictate the effective cloud area at the test section. The effective cloud area for these tests is approximated to be 0.46 m^2 (equivalent 30-in diameter) of the 0.66 m^2 (equivalent 36-in diameter) of the PSL test section area.

$$TWC_{target} = \frac{\dot{m}_{water}}{V_{air} AREA} \qquad (1)$$

From herein the TWC_{target} and *TWC* will be used synonymously.

In these set of test cases, both city water (filtered but untreated) and deionized water were used in the atomizing spray nozzles. The deionized water minimized the nucleation of ice crystals resulting in clouds that were entirely formed of liquid water droplets. Additionally, the cold air temperatures generated in these test cases produced supercooled liquid droplet clouds. City water was used in the lowest plenum pressure, P_{pl}, cases. To aid in the interpretation and analysis of the data, Table 1 provides a list of the cases presented in this section. Note that the air temperature was below the standard freezing point of water in all tests, while the water temperature was introduced at temperatures above freezing. In addition, the plenum relative humidity was maintained at nominally 45

The charts on the left side of Fig. 4 (namely, Figs 4a, 4c, 4e) show the changes in local total temperature, $\Delta T_{0,RFP}$, measured by the RFP for the range of *TWC* tested. In these charts, the plenum total pressure, P_{pl}, was maintained in a tight range and used as the main parameter, and likewise T_{pl} was kept in a tight range and used as a secondary parameter for individual plots within each chart. In this way, each chart represents the effects of one parameter at a time. The plenum temperatures and pressures were parametrized as follows: Low P_{pl}, 20 to 28 kPa; Mid P_{pl}, 62 to 70 kPa; and High P_{pl}, 90 to 97 kPa. However, not all temperature ranges were available for each pressure range. Ice crystal particle size or droplet size were within 15 to 20 µm in all these cases. The ubiquitous negative temperature changes found in these tests indicates a cooling of the airflow as a result of the interaction with the cloud. For clarity, since all the changes in total temperature were negative in this figure the descriptors such as "downward" or "dropped" are used to signify a negative increase in $\Delta T_{0,RFP}$ with increasing *TWC*, and therefore relatively cooler air temperatures at larger *TWC*. Likewise descriptors such as "upward" or "rise" are used to indicate a decrease in the negative values of $\Delta T_{0,RFP}$, i.e. a diminished cooling effect at increasing *TWC*. On the right side of Fig. 4 are the plots of the corresponding humidity measurements (Figs. 4b, 4d, and 4f). Humidity measurements are given in terms of the Mass Mixing Ratio (*MMR*) with units of grams of water vapor/kg of air, and the variable Δ*MMR* refers to the change in *MMR* values between the pre-spray value and the steady-state value during spray activation. A positive increase in *MMR* indicated an increase in the amount of water vapor transferred to the main airflow, and the magnitude of the slope of Δ*MMR* with respect to *TWC* indicated the rate of increase in water vapor. The different plenum total pressure cases are presented below.

Low plenum total pressure

Figure 4a shows the effects of the cloud at the lowest P_{pl} case in which city water was used to form fully glaciated clouds. These conditions resulted in temperature drops, or cooling of the air, by -1.2 to -2.8 ºC from an interaction with the cloud. The temperature drops were larger at the higher plenum temperature (T_{pl} of -4 to -2 ºC) compared to the lower plenum temperature (-11 to -8 ºC). Above a *TWC* value of 2 g/m^3, $\Delta T_{0,RFP}$ rose indicating that at higher total water content resulted in a smaller cooling effect of the air. In comparison, the thermal model data showed somewhat different values and trends. In this case, the modeling data showed a rapid rise in $\Delta T_{0,RFP}$, with values above the test data and going to positive values at a *TWC* of about 2 g/m^3. The humidity measurements plotted in Fig. 4b shows Δ*MMR* increased with *TWC*. While this case showed the least agreement between modeled and measured $\Delta T_{0,RFP}$, it provided the best agreement for Δ*MMR*. The modeling data clearly exhibits two stages of rising humidity: a rapid rise for *TWC* of 0 to 2 g/m^3, and a considerably slower rise thereafter. No experimental data was obtained at *TWC* values associated with the rapid rise in the modeling data for a comparison.

Mid plenum total pressure

The mid P_{pl} case (Fig. 4b) (as well as the high P_{pl}) was performed using DI droplet cloud. This case produced $\Delta T_{0,RFP}$ between -0.7 to -1.5 ºC and Δ*MMR* of 0.46 to 1.3 g/kg. The $\Delta T_{0,RFP}$ and Δ*MMR* experimental data at the two plenum temperatures were similar. This case also exhibited and inflection point where $\Delta T_{0,RFP}$ drops in value initially and then rises above a *TWC* of 2 g/m^3. The modeling data for this case of P_{pl} showed a closer fit to the test data. The humidity data in this case showed a characteristic transition in Δ*MMR* from low to high *TWC* at a *TWC* of 2 g/m^3, where Δ*MMR* rises rapidly in the low *TWC* range and then the rise tapers off or even steadies out after this transition point.

High plenum total pressure

The high P_{pl} case was characteristically similar to the mid P_{pl} case. The values in $\Delta T_{0,RFP}$ ranged between -0.6 to -2.0 ºC and in ΔMMR between 0.46 to 1.5 g/kg. This case also showed a downward trend in $\Delta T_{0,RFP}$ with increasing TWC. However, the measured $\Delta T_{0,RFP}$ did not increase with further increases in TWC as observed in the mid TWC case. There was a little more spread in the test data at the larger *TWC*. The modeled $\Delta T_{0,RFP}$ data was in close agreement with the test data. However, the modeling data still showed an inflection point, although a little more subtle than in the mid P_{pl} case, which was not seen in the test data. The humidity measurements at the different plenum temperatures were similar at each TWC, except for one point at low TWC, and were in close agreement with the modeling data.

Table 1: List of experimental test cases in Figure 4.

Figure	Plenum Pressure (P_{pl}) [kPa]	Plenum Temp. (T_{pl}) [ºC]	Parameter in plots	Particle MVD [µm]	Mach	Tw [ºC]	City/DI water	RH %
4a,b	low: 20 to 28	low, mid, high*	Temp	15 - 20	0.44	7.2	City	45
4c,d	mid: 62 to 70	low, mid, high*	Temp	15 - 20	0.22	82	DI	45
4e,f	high: 90 to 97	low, mid, high*	Temp	15 - 20	.13 - .22	82	DI	45

*Low T_{pl}, -11 to -8 ºC; Mid T_{pl}, -6 to -5 ºC; and High T_{pl}, -4 to -2 ºC.

Analysis

The results shown in Figures 4 illustrate the thermal interaction effects between the main air flow and the initially warm liquid droplet cloud. Based on the present data, evaporative heat transfer, specifically cooling, seems to be the dominant heat transfer mechanism in all the cases of Fig. 4. It is more pronounced in the low total pressure and highest total temperature cases shown in Fig. 4a because: 1) the lower pressure and higher temperatures promote faster evaporation, and 2) because the lower density results in lower thermal mass or inertia of the air, thereby causing the air to be more sensitive and react more quickly to the level of evaporation taking place. In the higher total pressure cases, these evaporation favorable conditions are somewhat diminished and result in smaller temperature decreases as found in the present data. With sufficient amounts of evaporation and/or static temperature decreases, the air can become saturated (RH = 100%) as a volume of air travels along the tunnel to the test section. When the air is near or at saturation, evaporation is reduced. So whereas the addition of greater water content to the air may not cause much more evaporation to occur when at or near saturation, it can add extra thermal energy to the air via convection. The convective heating which dominates this phase of the interaction causes increases in the air temperature due to the initially warm water (7.2 ºC or 82 ºC) of the spray and can explain the upward trend in total temperature changes with higher *TWC*, producing the inflection point found in the test and modeling data. The water droplets not only lose sensible energy to the air but also latent energy of fusion if any freezing occurs. With little more evaporation that occurs near saturation, any additional warm water adds energy into the control volume of air. The low pressure case in Fig. 4a exhibits this effect well. When the temperature of the free stream air is lowered, its capacity to contain water vapor is reduced, thereby decreasing the amount of evaporative cooling. This might explain the slightly smaller $\Delta T_{0,RFP}$ values at the lower T_{pl} plots. Whereas, in the high P_{pl} case in Fig. 4a, the generally small temperature drops and varying trend found here could have been a result of the different influences that the evaporative and convective heat transfer processes impart on the airflow at these pressures. While the rate of evaporation is lower at these higher atmospheric pressures, the denser air also resulted in larger thermal mass for convective heating.

The same line of reasoning holds in terms of humidity change generated in the icing cloud and airflow interaction. The largest increases in *MMR* were measured under the combined lowest plenum pressure and highest temperature conditions. Again, this indicates that at these conditions, the largest level of evaporative cooling takes place, which is manifested by the largest drop in total temperature and largest increases in humidity. At the lowest P_{pl}, the ice cloud is fully glaciated due to the use of city water, and led to greater amount of evaporation for the same *TWC* than in the higher total pressure cases. Again, this seemed to be case at the highest total temperature case as well.

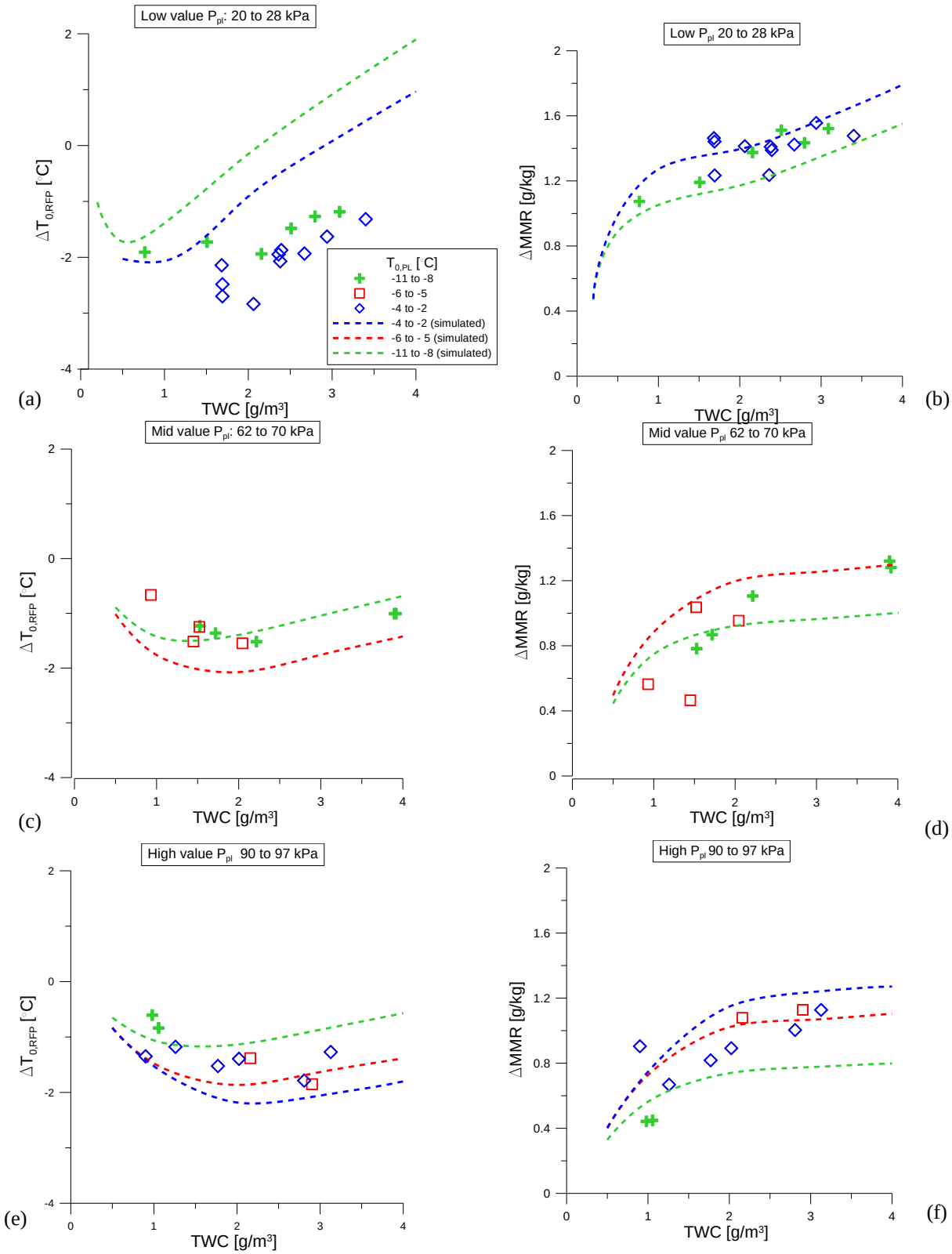

Figure 4: Plots of $\Delta T_{0,RFP}$ and ΔMMR. Cases: (a) $\Delta T_{0,RFP}$ vs *TWC* for low P_{pl}, (b) ΔMMR vs *TWC* for low P_{pl} (c) $\Delta T_{0,RFP}$ vs *TWC* for mid P_{pl} (d) ΔMMR vs *TWC* for mid P_{pl} (e) $\Delta T_{0,RFP}$ vs *TWC* for high P_{pl}; and (f) ΔMMR vs *TWC* for high P_{pl}

VII. Select Cases of Air Temperature Rise through interaction with the Ice Cloud

In the previous section, all experimental test points presented measured a decrease in air temperature at the test section when an icing cloud was activated. Five select cases are presented in this section where air temperature at the test section increased in the presence of an icing cloud. Previous evaluations of the Bartkus thermal model only compared simulation results with experimental results where only air temperature decreased. These comparisons will test the model in a new set of conditions.

Table 2 shows the conditions for the five tests cases where an increase in air temperature was measured. These five cases represent all of the test runs where air temperature increased in the entire matrix of tests. Unlike the previous section where parametric sweeps were analyzed, the conditions for these five cases are more stand-alone as various parameters vary. Despite the variance in conditions between cases, a few parameters are identified as important for why an air temperature increase was measured. An important distinction is that four of the five cases were run at low pressures (P_{pl} =~22 kPa). Whereas total air temperature is below freezing for all tests, two of the cases (test runs # 214 and 216) are colder than the rest and more than 20 ºC below freezing. Also, in addition to being run with unconditioned (city) water, all tests were run with *TWC* values of 4.7 g/m^3 and higher, which are higher *TWC* values than in the previous section where air temperature decreased with cloud activation. The *TWC* values shown in Table 2 represent the water content expected at the test section assuming no vaporization of the cloud.

Figure 5 shows comparisons between experimental data and simulation results of temperature changes and vapor content changes for the five select cases. The Bartkus thermal model simulation results agree well with experimental temperature and vapor content measurements. Model results suggest that temperature increases occurred due to several factors. Whereas water injected into the wind tunnel undergoes evaporation, which reduces air temperature, water warmer than the flowing air temperature drives energy exchange towards the air via convective heat transfer. More sensible and latent energy is introduced into the air control volume of the icing wind tunnel as greater water contents are injected. The amount that can be vaporized is limited by the air temperature. Once the air becomes saturated, larger amounts of *TWC* injected into the tunnel do not result in more evaporation and greater decreases in air temperature, but rather reduced air temperature decreases as sensible and latent heat is transferred to the air. If enough water is injected at temperatures warmer than the air, eventually air temperature will increase in the presence of a cloud.

The largest increases in air temperature occurred when initial air temperature and pressure were lowest. Lower air temperatures increase the amount of sensible energy that is transferred to the air, along with all of the latent heat of fusion -as the liquid water glaciates. Also, lower air temperatures reduce the amount that water can vaporize, reducing the amount that evaporative energy transfer can remove from the air. Test run # 216 was run at the coldest air temperature, which resulted in the smallest vapor increase, due to the low capacity to vaporize at this low temperature, but also saw a large temperature increase due to the sensible and latent energy transfer. Finally, low air pressures means that there is less air mass for a given control volume, thus any energy transferred will result in larger temperature changes, compared to higher air pressure tests.

Table 2: Test conditons for select set of test points producing positive $\Delta T_{0,RFP}$

Test Run	T_{PL} (total)	P_{PL} (total)	RH_{PL} (Total)	Exit Air Velocity	Target TWC	Approx Initial MVD	Water Type	Initial Water Temp
#	[^{O}C]	[kPa]	[%]	[m/s]	[g/m^3]	[µm]	[City/DI]	[^{O}C]
201	-3.1	22.5	45	144	6.52	33	City	8
214	-23.7	21.5	45	101	9.26	33	City	8
216	-35.7	23.9	45	128	4.70	41	City	8
304	-3.2	22.5	45	142	6.39	45	City	8
313	-15.7	86.6	45	115	6.45	24	City	8

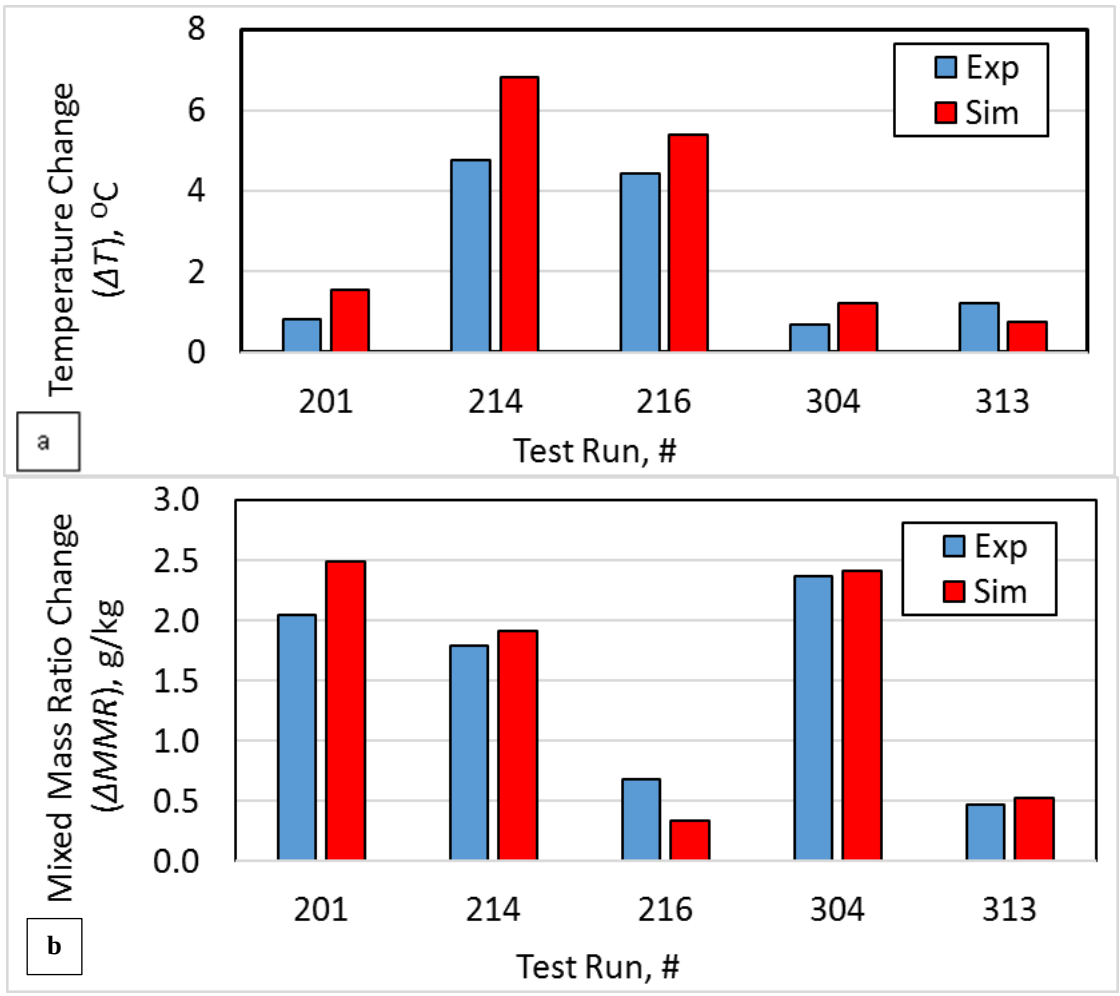

Figure 5: Test and model data comparison for select set of test points producing positive $\Delta T_{0,RFP}$.

VIII. Conclusion

A Rearward Facing Probe is being developed in-house to measure local total temperature and humidity during atmospheric icing flow conditions. The probe was recently used in a series of ice cloud characterization tests in the PSL which provided a sizeable dataset used to characterize the icing cloud effects on the main flow. Insight was gained from the parametric data analysis and associated thermal modeling of the interaction. The large temperature differential between the injected droplet and the atmospheric flow produced competing evaporative and convective heat transfer effects. The trends seen in sweeps of *TWC* showed that the changes in total temperature and humidity were sensitive to aerothermal conditions of the flow and the composition of the ice cloud. The conditions in the present data set generally produced small total temperature drops in the range of 0.6 to 2.8 ºC and up to 1.5 g/kg of water vapor rise through the interaction. The largest changes in total temperature and humidity generally occurred at plenum conditions of low pressure and high temperature, and under glaciated cloud conditions. The least effects were found at large *TWC* and low temperatures. Under certain very low temperature or high *TWC* conditions, the interaction with the cloud produced a warming of the airflow. The competing mechanisms of evaporative and convecting heat transfer, inherent in the thermal model, were helpful in interpreting these trends.

References

[1] Mason, J. G., Strapp, J. W., and Chow, P., "The Ice particle Threat to Engines in Flight," 44th AIAA Aerospace Sciences Meeting and Exhibit, AIAA, Reno, NV, 2006, AIAA-2006-206.

[2] Struk, P.M., Tsao, J.C. and Bartkus, T. (2016). Plans and Preliminary Results of Fundamental Studies of Ice Crystal Icing Physics in the NASA Propulsion Systems Laboratory. 8th AIAA Atmospheric and Space Environments Conference. Washington, DC, American Institute of Aeronautics and Astronautics. Paper AIAA-2016-3738
[3] Struk, P.M., Bartkus, T.P., Bencic, T.J., King, M.C., Ratvasky, T.P., Van Zante, J.F. and Tsao, J.C . (2017). An Initial Study of the Fundamentals of Ice Crystal Icing Physics in the NASA Propulsion Systems Laboratory. 9th AIAA Atmospheric and Space Environments Conference, American Institute of Aeronautics and Astronautics. AIAA-2017-4242
[4] Fuleki, D., et al. (2014). Development of a Sensor for Total Temperature and Humidity Measurements under Mixed-Phase and Glaciated Icing Conditions. 6th AIAA Atmospheric and Space Environments Conference, American Institute of Aeronautics and Astronautics. AIAA-2014-2751
[5] Bartkus, T. P., Struk, P. M., Tsao, J. C., and Van Zante, J. F. "Numerical Analysis of Mixed-Phase Icing Cloud Simulations in the NASA Propulsion Systems Laboratory," 8th AIAA Atmospheric and Space Environments Conference, AIAA-2016-3739, Washington D.C., 2016.
[6] Bartkus, T. P., Struk, P. M., and Tsao, J.-C. "Comparisons of Mixed-Phase Icing Cloud Simulations with Experiments Conducted at the NASA Propulsion Systems Laboratory," 9th AIAA Atmospheric and Space Environments Conference. American Institute of Aeronautics and Astronautics, Denver, CO, 2017.
[7] Van Zante, J. F., et al. (2018)" Update on the NASA Glenn Propulsion Systems Lab Icing and Ice Crystal Cloud Characterization (2017)" 10th AIAA Atmospheric and Space Environments Conference, AIAA Aviation Forum, 25–29 June 2018, Atlanta, GA (submitted for publication).
[8] Van Zante, J. F., et al. (2016). NASA Glenn Propulsion Systems Lab Ice Crystal Cloud Characterization Update 2015. 8th AIAA Atmospheric and Space Environments Conference. Washington, DC, American Institute of Aeronautics and Astronautics. AIAA-2016-3897
[9] Bartkus, T. P., Struk, P. M., and Tsao, J. C. "Development of a Coupled Air and Particle Thermal Model for Engine Icing Test Facilities," SAE Int. J. Aerosp. Vol. 8, No. 1, 2015. p. 18.Vatistas, G. H., Lin, S., and Kwok, C. K., “Reverse Flow Radius in Vortex Chambers,” *AIAA Journal*, Vol. 24, No. 11, 1986, pp. 1872, 1873.